

Imaging Receptor-Mediated Endocytosis with a Polymeric Nanoparticle-Based Coherent Anti-Stokes Raman Scattering Probe

Ling Tong,[†] Yanhui Lu,[‡] Robert J. Lee,[‡] and Ji-Xin Cheng^{*,†,§}

Department of Chemistry, Purdue University, West Lafayette, Indiana 47906, Division of Pharmaceutics, College of Pharmacy, The Ohio State University, Columbus, Ohio 43210, and Weldon School of Biomedical Engineering, Purdue University, West Lafayette, Indiana 47906

Received: May 7, 2007; In Final Form: June 19, 2007

Coherent anti-Stokes Raman scattering (CARS) microscopy was used to visualize receptor-mediated endocytosis and intracellular trafficking with the aid of a CARS probe. The probe was made of 200-nm polystyrene particles encapsulated in folate-targeted liposomes. By tuning ($\omega_p - \omega_s$) to 3045 cm^{-1} , which corresponds to the aromatic C–H stretching vibration, the polystyrene nanoparticles with a high density of aromatic C–H bonds were detected with a high signal-to-noise ratio, while the epi-detected CARS signal from cellular organelles was cancelled by the destructive interference between the resonant contribution from the aliphatic C–H vibration and the nonresonant contribution. Without any photobleaching, the CARS probe allowed single-particle tracking analysis of intracellular endosome transport. No photodamage to cells was observed under the current experimental conditions. These results show the advantages and potential of using a CARS probe to study cellular processes.

Introduction

With the development of fluorescent probes and realization of three-dimension (3D) resolution by confocal detection¹ or two-photon excitation,² fluorescence microscopy has become a powerful and widely used bio-imaging tool.³ However, most fluorophores are prone to photobleaching, which makes continuous observation of biological processes difficult. Recently, semiconductor quantum dots were developed as bright and photostable fluorophores to alleviate the photobleaching problem.^{4,5} The big challenge for quantum dots is the cytotoxicity due to the release of Cd²⁺ or Se²⁻ ions. Deleterious effects of quantum dots on embryo development⁶ and cell viability⁷ have been observed. Therefore, development of novel imaging probes is still greatly needed.

In this paper, we report a coherent anti-Stokes Raman scattering (CARS) probe for 3D imaging of cellular processes without photobleaching. CARS is a third-order nonlinear optical process in which a pump field E_p (ω_p) and a Stokes field E_s (ω_s) interact with a sample and generate an anti-Stokes field E_{as} at the frequency of $\omega_{as} = (\omega_p - \omega_s) + \omega_p$. The CARS signal can be significantly enhanced when ($\omega_p - \omega_s$) is tuned to a Raman-active vibrational band, which provides the vibrational contrast. Besides the molecular selectivity, CARS microscopy offers several other advantages summarized as follows. The CARS frequency is higher than the excitation frequencies and can thus be detected in the presence of one-photon-induced fluorescence. The temporally and spatially overlapping pump and Stokes laser pulses are tightly focused into a sample to generate a signal in a small excitation volume ($<1\ \mu\text{m}^3$), which produces inherent 3D spatial resolution. The coherent addition of CARS fields builds up a large signal, allowing high-speed

imaging from 1 frame per second⁸ to video rate.⁹ Last, because the generation of CARS does not necessitate electronic resonance, the photobleaching problem encountered in fluorescence microscopy can be eliminated.

Continuous technical developments in the last past few years have made CARS microscopy a mature image technique^{10,11} ready for biological and biomedical applications. CARS microscopy has been applied to label-free imaging of lipid bodies in live cells and skin tissues,⁹ and the myelin sheath in ex vivo spinal tissues¹² and in vivo sciatic nerves.¹³ By use of epi-detection that rejects the nonresonant background from the solvent,^{14,15} quantitative detection of a specific lipid in single bilayers was demonstrated.^{16–18} Dynamic processes including intracellular hydrodynamics¹⁹ and lipid droplets trafficking in cells²⁰ were investigated by CARS microscopy as well. In several in vitro studies, deuterated lipids were used for CARS imaging of specific lipid molecules in single lipid bilayers.^{17,21,22} However, imaging a cellular process (i.e., endocytosis) with a CARS probe has not been reported.

In this study, we use a polymeric nanoparticle-based CARS probe to follow folate-receptor-mediated endocytosis and intracellular trafficking of endosomes. Folate receptor is a highly selective tumor marker that brings cargoes into tumor cells via receptor mediated endocytosis.^{23,24} Various folate-conjugated drug carriers including folate-targeted liposomes^{25–27} have been designed to be transported into cells through a folate receptor dependent pathway. A common way to visualize the folate-targeted liposomes is to encapsulate a hydrophilic fluorescent dye such as calcein²⁶ into the liposomes. Although this method allowed flow cytometry detection, it is difficult to follow the cellular uptake and intracellular trafficking process because of the photobleaching of the encapsulated fluorescent probes. To alleviate this problem, we loaded the folate-targeted liposomes with polystyrene nanoparticles to follow folate receptor mediated endocytosis in KB cells by CARS microscopy. Because of the high density of aromatic C–H bonds in polystyrene, sample-

* Corresponding author. E-mail: jcheng@purdue.edu.

[†] Department of Chemistry, Purdue University.

[‡] The Ohio State University.

[§] Weldon School of Biomedical Engineering, Purdue University.

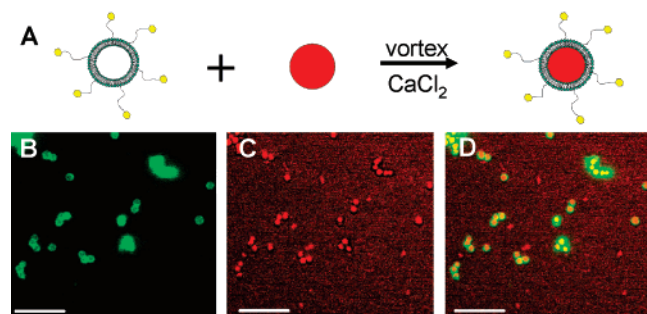


Figure 1. Encapsulation of melamine beads into folate-targeted liposomes. (A) Scheme for preparation of folate-targeted liposomes encapsulated with melamine beads. (B) DiOC18 signal (green) in lipid bilayers taken by confocal fluorescent microscopy with a 488-nm Ar^+ laser. (C) F-CARS signal (red) of 1.0- μm melamine beads with $(\omega_p - \omega_s)$ at 2840 cm^{-1} . (D) Overlay of simultaneous acquired F-CARS (red, beads) and epi-fluorescence (green, DiOC18 in lipid bilayers) images indicated that lipid bilayers were coated on the bead surface. Length bar = $10\ \mu\text{m}$.

scanning²⁸ and laser-scanning⁸ CARS imaging of polystyrene nanoparticles as small as 100 nm has been demonstrated. More importantly, by tuning $(\omega_p - \omega_s)$ to 3045 cm^{-1} , the peak frequency of the CARS band for aromatic C–H stretching vibration, the CARS signal from cellular organelles can be canceled by the destructive interference between the aliphatic C–H vibration and the nonresonant background. These properties allowed selective imaging of receptor mediated uptake of polystyrene nanoparticles without photodamage to KB cells.

Experimental Section

Materials. Hydrogenated soy phosphatidylcholine (HSPC), dipalmitoyl phosphatidylcholine (DPPC), cholesterol, and methoxy-polyethylene glycol (MW 2000)-distearoyl phosphatidylethanolamine (mPEG-DSPE) were purchased from Avanti Polar Lipids (Alabaster, AL). Folate-PEG-cholesterol was synthesized as described previously.²⁹ Melamine beads ($1.06 \pm 0.06\ \mu\text{m}$ in diameter, 2.51% solids) and polystyrene nanoparticles ($0.202 \pm 0.010\ \mu\text{m}$ in diameter, 2.62% solids) were purchased from Polysciences Inc (Warrington, PA).

Preparation of Liposomes Loaded with Calcein or Particles. Folate-targeted liposomes loaded with calcein were prepared by the polycarbonate membrane extrusion method.²⁹ Briefly, HSPC, cholesterol, mPEG-DSPE, and folate-PEG-cholesterol were co-dissolved in chloroform at a molar ratio of 55:40:4.5:0.5. The lipid mixture was dried under N_2 to form a thin film in a glass tube and vacuumed overnight. The dried lipid was hydrated in 1 mL of phosphate-buffered saline (PBS) supplemented with 12.5 mM calcein, sonicated, and then extruded 21 times through a 50 nm pore-size polycarbonate membrane using a manual extruding device (Avanti) at $65\text{ }^\circ\text{C}$. To remove the free calcein, liposomes were purified on a PD-10 desalting column (GE Healthcare). The diameter of liposomes was determined to be $115.46 \pm 26.18\text{ nm}$ by dynamic light scattering (DLS, DynaPro 99, Protein solutions).

Liposomes encapsulating particles were prepared by following the method of Galneder et al.³⁰ First, liposomes containing DPPC and cholesterol at a molar ratio of 9:1 ($3\ \mu\text{mol/mL}$ in chloroform) were prepared by the above-described extrusion method. For folate-targeted liposomes, 0.5% folate-PEG-cholesterol was added to the chloroform solution of lipid mixture. Instead of using calcein-containing PBS, 1 mL of milli-Q water was added to hydrate the dried lipid. The diameter of liposomes was determined to be 68–80 nm by DLS. The

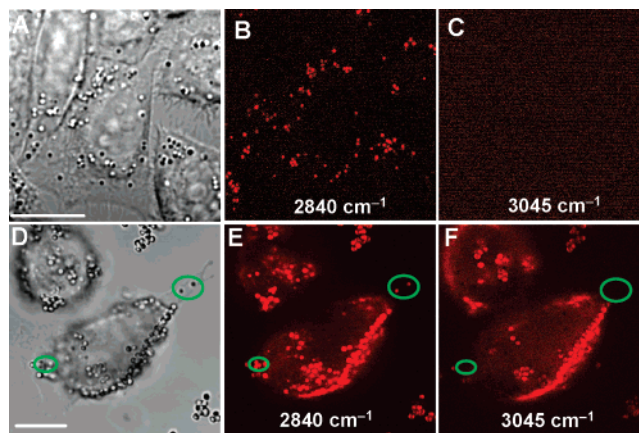


Figure 2. Selective imaging of melamine beads attached to KB cells by E-CARS microscopy. (A–C) Transmission and E-CARS images of a KB cell. (A) Transmission image. (B) E-CARS signals from lipid droplets in the same cell with $(\omega_p - \omega_s)$ at 2840 cm^{-1} (red dots). (C) No E-CARS signal was probed from organelles in the same cell with $(\omega_p - \omega_s)$ at 3045 cm^{-1} . (D–F) Transmission and E-CARS images of a KB cell with high binding of 1.0- μm melamine beads encapsulated in folate-targeted liposomes. (D) Transmission image of KB cells and beads. (E) Cells seen by E-CARS with $(\omega_p - \omega_s)$ at 2840 cm^{-1} (red dots). Both organelles (typically indicated in the green circle) and beads were visualized. (F) Cells seen by E-CARS with $(\omega_p - \omega_s)$ at 3045 cm^{-1} (red dots). Only beads were visualized by E-CARS with $(\omega_p - \omega_s)$, and no signal from organelles was observed. The pump and Stokes laser wavelengths were tuned to 713 and 893 nm with $(\omega_p - \omega_s)$ at 2840 cm^{-1} , or 703 and 893 nm with $(\omega_p - \omega_s)$ at 3045 cm^{-1} . Length bar = $10\ \mu\text{m}$.

freshly prepared liposomes were mixed with 0.1 mL of melamine beads or polystyrene nanoparticles. CaCl_2 at $1\text{--}2\ \mu\text{M}$ was added to promote fusion of liposomes onto the beads or nanoparticles. The particles were then allowed to sediment overnight and the supernatant was replaced with 1 mL of milli-Q water. To check whether the particles were coated with lipid bilayers, 1% DiOC18 was added during liposome preparation and 20 μL of the labeled particles was dropped on a coverslip and simultaneously imaged by CARS and fluorescent microscopy.

Cell Culture and Treatment. KB cells, a folate receptor positive epidermal carcinoma cell line, were cultured at $37\text{ }^\circ\text{C}$ in a humidified atmosphere containing 5% CO_2 and grown continuously in folate-deficient RPMI 1640 medium (Invitrogen) containing 10% fetal bovine serum (FBS, Sigma) and 1% penicillin-streptomycin (Invitrogen). In a typical experiment, a 1-mL suspension of KB cells (10^5 cells/mL) was plated onto a coverslip-bottom Petri dish (MatTek), grown for 2–3 days, then treated with 60 μL of liposomes encapsulated with nanoparticles and maintained at $37\text{ }^\circ\text{C}$ with periodic monitoring.

Laser-Scanning CARS Microscopy. A schematic of our laser-scanning CARS microscope has been presented in a previous report.¹² The pump and Stokes laser beams were generated by two tightly synchronized (Sync-Lock, Coherent) Ti:sapphire oscillators with a pulse width of 2.5 ps (Mira 900, Coherent Inc., Santa Clara, CA). The two beams were collinearly combined with a dichroic combiner (LWP-45-R720-7850-PW-1004-UV, CVI Laser LLC, Albuquerque, NM). A Pockels' cell (model 350-160, Conoptics, Danbury, CT) was used to reduce the repetition rate to 3.9 MHz. The average power at the sample was about 4.8 mW. The combined laser beams were directed into a laser-scanning confocal microscope (FV300/IX70, Olympus America Inc., Melville, NY). A $60\times$ water immersion objective (1.2 numerical aperture (NA)) was used to focus the excitation beams into the sample. Forward-CARS (F-CARS)

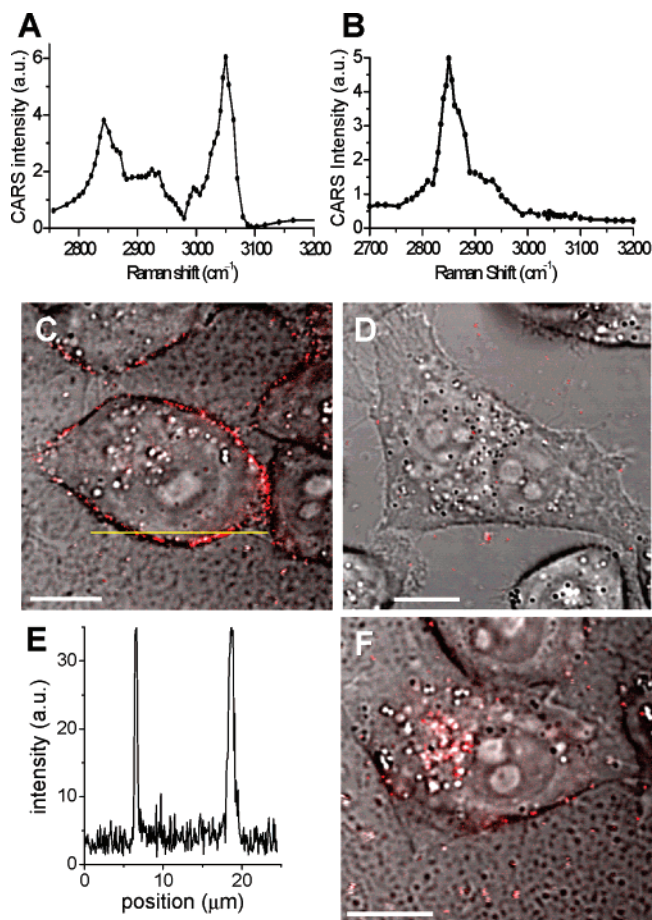


Figure 3. E-CARS imaging of cellular uptake of 200-nm polystyrene nanoparticles encapsulated in folate-targeted liposomes. (A) CARS spectrum of polystyrene, adapted from an earlier paper.⁴¹ (B) CARS spectrum of a single lipid droplet inside a KB cell. (C) After 2-h incubation, 200-nm polystyrene nanoparticles encapsulated in folate-targeted liposomes (red) strongly bound to the KB cell surface. (D) Polystyrene nanoparticles encapsulated in non-folate-targeted liposomes showed no binding to cell surface after 2-h incubation. (E) Intensity profile for a linescan in Figure 3C showed a high signal-to-background ratio for the 200-nm nanoparticles. (F) After 7-h incubation, the 200-nm nanoparticles were internalized into KB cells and delivered to a perinuclear area. All images were taken with $(\omega_p - \omega_s)$ at 3045 cm^{-1} . Length bar = $10\ \mu\text{m}$.

signals were collected by an air condenser (0.55 NA) and detected with a photomultiplier tube (PMT, R3896, Hamamatsu, Hamamatsu City, Japan). Epi-detected CARS (E-CARS) signals were collected by the same objective, spectrally separated from the excitation source by a dichroic mirror (670dxcr, Chroma Technology Corp., Rockingham, VT), transmitted through a bandpass filter (42-7336, Ealing Catalog Inc., Rocklin, CA), and detected by a PMT (H7422-40, Hamamatsu, Hamamatsu City, Japan) installed at the back port of the microscope.

Single-Particle Tracking (SPT) Analysis. FluoView software (Olympus, Tokyo, Japan) was used to convert time-lapse CARS images to a series of 8-bit TIFF files. The SPT code developed by Crocker and Grier³¹ was modified in our lab by using the IDL language to track multiple “Gaussian-like” blobs which mimic the particles moving in live cells. The image pixel sizes were adjusted to a spatial resolution suitable for tracking individual particles, which could be readily identified after appropriate parametrization of particle size, eccentricity, and total and mean intensities. The centroid of a given particle could be determined with sub-pixel resolution by fitting its intensity profile to a Gaussian distribution; trajectories were produced

by correlating changes in centroid positions between adjacent frames. Particle movement was characterized by its instantaneous velocity, calculated as the displacement divided by the time interval between two adjacent frames. Plus and minus velocities were used to indicate movement toward the cell periphery and the nucleus, respectively. The mean squared displacement (MSD) was calculated as a function of the lag time (Δt) and fitted according to the diffusion plus directed motion equation, describing active transport of particles: $\text{MSD} = 4D\Delta t + (v\Delta t)^2$, where D is the diffusion coefficient and v is the average velocity.

Results and Discussion

A CARS probe was prepared by encapsulation of particles into liposomes. The encapsulation was accomplished by fusion of liposomes onto particles with the aid of CaCl_2 , as shown in Figure 1A. To check whether the particles have been coated with lipid bilayers, DiOC18 was integrated in the lipid membrane for visualization of the bilayers and sizable $1.0\text{-}\mu\text{m}$ melamine beads were used for microscopic examination. After sedimentation and resuspension with milli-Q water, $20\ \mu\text{L}$ of a solution of liposomes encapsulated with melamine beads was dropped and dried on a coverglass. Lipid bilayers and beads were simultaneously imaged by epi-fluorescence and F-CARS, respectively. The green rings in Figure 1B were the fluorescent signals from DiOC18 in the lipid bilayer, generated by 488-nm Ar^+ laser. The red spots in Figure 1C were F-CARS signals from melamine beads with $(\omega_p - \omega_s)$ at 2840 cm^{-1} . The complete overlay of the red spots inside the green rings (Figure 1D) indicated that the lipid bilayers were indeed coated on the beads.

Two issues must be considered when developing a CARS probe for cellular studies. The first is the nonresonant background from the bulk solvent that limits the image contrast and spectral selectivity. This problem can be alleviated by using E-CARS, which provides a high contrast for small objects by rejecting the background from bulk solvent.^{14,15} The second is that cellular organelles, enriched in aliphatic C–H bonds, exhibit a bright contrast in E-CARS images with $(\omega_p - \omega_s)$ tuned to 2840 cm^{-1} . Therefore, a strategy that weakens the organelles’ signals but enhances the probe’s signal is needed.

To eliminate the signal from the cellular organelles, we tuned $(\omega_p - \omega_s)$ to 3045 cm^{-1} , the CARS peak for aromatic C–H stretching vibration. At this frequency, the E-CARS signal from cellular organelles was canceled by the destructive interference between the resonant contribution from the aliphatic C–H vibration and the nonresonant contribution (Figure 2A–C). We further explored the detection of melamine beads encapsulated in folate-targeted liposomes under the same condition. After 2-h incubation in cells, transmission (gray, Figure 2D) and E-CARS (red, Figure 2E,F) images of the same KB cell were taken at different CARS peaks. At 2840 cm^{-1} (Figure 2E), both organelles (red dots indicated in green circles) and melamine beads were clearly seen by E-CARS, making it difficult to distinguish them from each other. At 3045 cm^{-1} (Figure 2F), no E-CARS signal from cellular organelles was detectable due to the destructive interference, while a strong nonresonant E-CARS signal from melamine beads (no C–H bonds) was observed. Therefore, combination of epi-detection with tuning $(\omega_p - \omega_s)$ to 3045 cm^{-1} allowed us to monitor the CARS probes without any background from cell organelles and water.

Though the $1.0\text{-}\mu\text{m}$ melamine beads encapsulated in folate-targeted liposomes were observed to strongly bind to the KB cell surface after 2-h incubation (Figure 2D–F), it was difficult

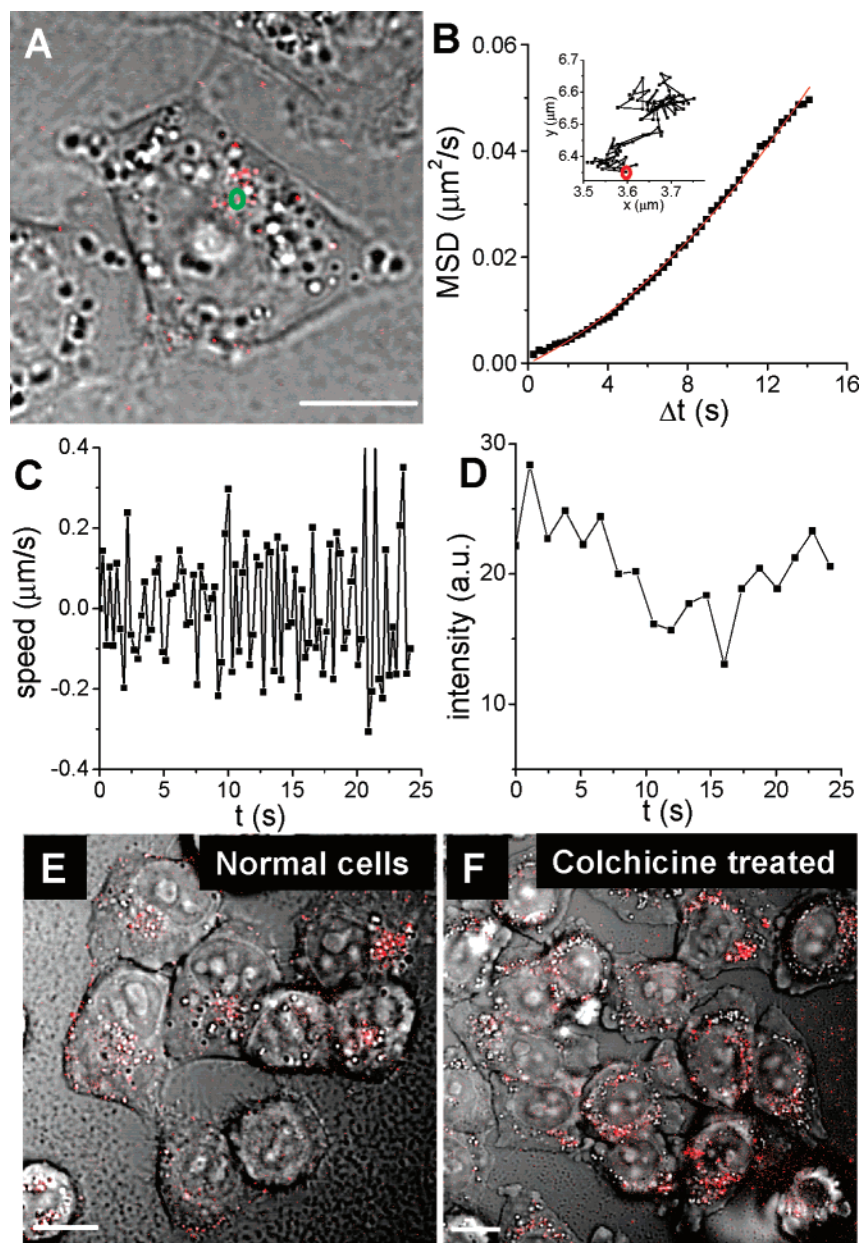


Figure 4. Intracellular trafficking of endocytosed 200-nm nanoparticles in KB cells. (A) E-CARS image of internalized 200-nm nanoparticles (red) after 7-h incubation. The nanoparticle being tracked was highlighted by a green circle. (B) Mean squared displacement (MSD) of nanoparticle signal (squares). Least-squares fit (solid curve) described active intracellular transport according to the function $MSD = 4D\Delta t + (\nu\Delta t)^2$ where D is the diffusion coefficient and ν is the average transport speed. $D = 460 \text{ nm}^2/\text{s}$; $\nu = 11.4 \text{ nm/s}$. Inset: nanoparticle trajectory in KB cell over a 25-s period. The red circle indicated the starting point of the trajectory. (C) Instantaneous nanoparticle velocities over a 25-s period. Plus and minus velocities were used to indicate movement toward the cell periphery and the nucleus, respectively. (D) E-CARS intensity fluctuation of the tracked nanoparticle over the 25-s period. The fluctuation was due to temporary deviation from the focal plane during the endosome movement. (E) After 7-h incubation, 200-nm polystyrene nanoparticles (red) were internalized and delivered to a perinuclear area in the KB cells. (F) After treating the nanoparticles internalized cells with colchicines ($30 \mu\text{M}$) for 0.5 h to destroy the microtubule network, the nanoparticles were randomly distributed in the cytosol, further confirming their active transport along the microtubule. All images were taken with $(\omega_p - \omega_s)$ at 3045 cm^{-1} . Length bar = $10 \mu\text{m}$.

for them to be internalized due to their large size. Even after 7-h incubation, most of them remained on the cell surface (data not shown). To increase the internalization rate, we encapsulated into folate-targeted and non-folate-targeted liposomes 200-nm polystyrene particles. Although these particles were small, the abundant aromatic C–H vibration in polystyrene greatly enhanced the CARS signal acquired at 3045 cm^{-1} , as shown in Figure 3A. Meanwhile, the CARS signal from the cellular lipid at this Raman shift is canceled by the destructive interference between the aliphatic C–H vibration and the nonresonant background (Figure 3B).

After 2-h incubation of cells with the folate-targeted liposomes encapsulating polystyrene nanoparticles, we observed a strong E-CARS signal (red) from the polystyrene nanoparticles bound to KB cells (Figure 3C), while little CARS signal was observed in cells treated with non-folate-targeted liposomes (Figure 3D), indicating that the binding was specific to the folate receptor. Different from $1.0\text{-}\mu\text{m}$ melamine beads, 200-nm polystyrene nanoparticles were observed to be fully internalized and delivered to the perinuclear region after 7-h incubation (Figure 3F). Figure 3E showed the E-CARS intensity profile for a linescan in Figure 3C. The signal-to-noise ratio (SNR)

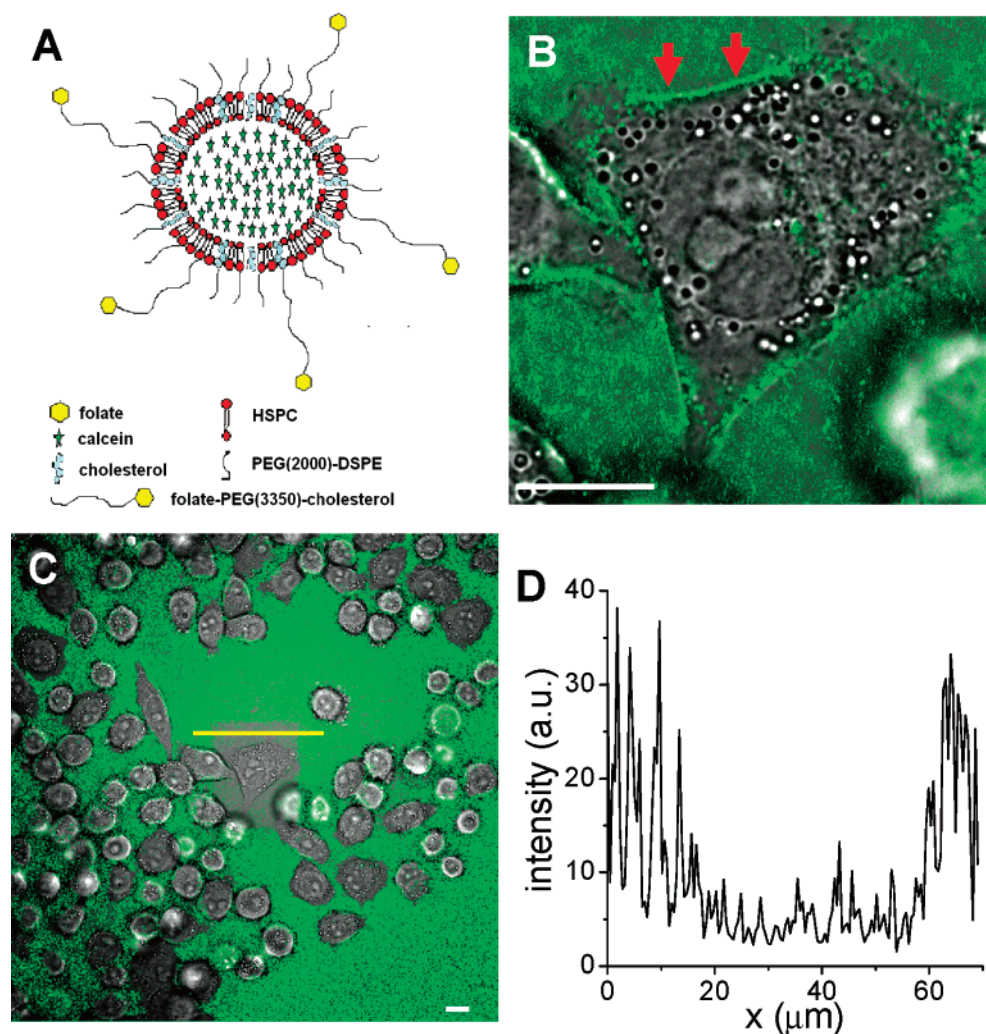


Figure 5. Fast photobleaching of calcein-loaded liposomes. (A) Structure of folate-targeted liposomes (HSPC/cholesterol/mPEG-DSPE/folate-PEG-cholesterol = 55:40:4.5:0.5 mol/mol, loaded with 12.5 mM calcein (before column), $d = 115.46 \pm 26.18$ nm). (B) After 0.5-h incubation with 70 μ L of folate-liposomes in 1 mL of KB cells at 37 $^{\circ}$ C, liposomes (green) strongly bound to KB cell surface (indicated by the red arrow). (C) Fast photobleaching of calcein after continuous imaging a single cell for 2.7 s (scan area 39.28 μ m \times 39.28 μ m). (D) Fluorescence intensity profile of calcein after photobleaching. The intensity decreased by about 80%. Length bar = 10 μ m.

was around 6, and the full width at half-maximum (fwhm) was around 0.25 μ m. Such high detection sensitivity and spatial resolution allowed us to study intracellular trafficking of the internalized particles.

We have monitored the trafficking of endocytosed 200-nm nanoparticles in KB cells using time-lapse E-CARS imaging. E-CARS movies of internalized nanoparticles over 25-s intervals were analyzed to determine their trajectories and instantaneous velocities. An example is shown in Figure 4A–C. The nanoparticle exhibited a bidirectional motion (Figure 4C) toward the nucleus (negative speed) and the cell membrane (positive speed). The mean squared displacements (MSD) (Figure 4B) were fully consistent with a directed motion model, with diffusion constant $D = 460$ nm²/s and average speed $v = 11.4$ nm/s. There was no CARS signal reduction during the 25-s period (Figure 4D). The intensity fluctuation was due to temporary deviation from the focal plane during the endosome movement. The directed transport of nanoparticles was likely along microtubules, as disruption of the microtubule network by colchicine caused the nanoparticles to be randomly distributed in the cytosol (Figure 4F), in contrast to the perinuclear accumulation in the normal cells (Figure 4E).

To showcase the advantage of using a CARS probe, we have examined the photostability of calcein loaded in the interior of

folate-targeted liposomes by confocal fluorescent microscopy. Calcein is a widely used hydrophilic fluorescent probe for liposome detection.²⁶ In contrast to the photostable CARS probe, the fluorescent intensity from calcein was reduced by 80% after continuous imaging of a single cell densely bound with folate-targeted liposomes for 2.7 s (Figure 5). The fast bleaching of fluorescence hampered its application to the study of intracellular transport. Therefore, a photostable imaging agent such as the CARS probe is needed.

We have characterized the photodamage to KB cells during the period of CARS imaging. Due to the high laser intensity at the focal center, photodamage to the biological sample is an important issue for multiphoton microscopy.^{32–34} Mechanisms of photodamage in CARS imaging of intact myelin sheath in spinal tissues and cultured cells have been studied.^{20,35,36} For the compact myelin sheath, both linear and nonlinear mechanisms were involved,³⁵ and the damage was enhanced by coherent-Raman-induced vibrational excitation.³⁶ For cultured cells, photodamage was featured by morphological changes, such as plasma membrane blebbing and cell retraction,^{20,35} and was found to be dominated by a second-order mechanism.³⁵ In the current study, we also considered the morphological change as an indicator of cell damage. With the pump and Stokes laser wavelengths tuned to 703 and 893 nm and pump and Stokes

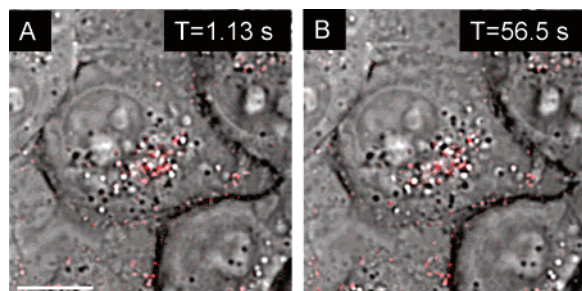


Figure 6. Characterization of photodamage during time-lapse CARS imaging of KB cells. (A) E-CARS image of a KB cell before laser scanning. (B) E-CARS image of the same KB cell after laser scanning. After 56.5-s scanning (1.13 s per scan) of an area of $36.36 \mu\text{m} \times 36.36 \mu\text{m}$ by E-CARS, no cellular morphology changed, indicating little photodamage to KB cells under the current experimental conditions. The pump and Stokes laser wavelengths were tuned to 703 and 893 nm. The average pump and Stokes laser powers were 3.96 and 0.84 mW, respectively. All images were taken with $(\omega_p - \omega_s)$ at 3045 cm^{-1} . Length bar = $10 \mu\text{m}$.

laser powers of 3.96 mW (1.02 nJ) and 0.84 mW (0.22 nJ) at the sample, respectively, no membrane blebbing or cell retraction were observed after scanning an area of $36.36 \mu\text{m} \times 36.36 \mu\text{m}$ for 56.5 s (1.13 s per scan). The cell remained in good shape, and the nanoparticles were clearly visualized without any burning (Figure 6). The power used in our work was lower than the nonlinear damage threshold (2 nJ for 711-nm beam) determined in the paper of Nan et al.²⁰ and the average power (9.24 mW for 1 min) used to induce cellular damage in an article by Fu et al.³⁵ Therefore, our experimental conditions were safe for CARS imaging of live cells over an extended period of time.

Finally, we compare the CARS probes with gold nanoparticles as imaging probes. The strong plasmon scattering from gold nanoparticles has been widely used for single-particle tracking studies by dark-field microscopy.³⁷ The dark-field contrast lacks the depth resolution and is not applicable to ex vivo and in vivo studies, while the CARS probes have the potential for 3D imaging of biological processes in both cellular and in vivo environments. Recently, a strong two-photon luminescence from gold nanorods was observed³⁸ and used for 3D imaging of cancer cells embedded in a collagen matrix.³⁹ As imaging agents, the CARS probes have two advantages over the gold nanorods. First, the two-photon luminescence emission spectrum of gold nanorods is very broad, making it difficult to co-localize the nanorods with other fluorophores. In contrast, the CARS spectral profile is determined by the picosecond excitation pulses in our case and has a width of less than 1 nm, which facilitates the co-localization study with other fluorescent dyes. Second, gold nanorods effectively convert the light energy to heat,⁴⁰ which may cause thermal injury of cells during the imaging process. On the contrary, as CARS is a four-wave mixing process during which little heat is produced, the CARS probes can be used with little damage to cells, as shown in our paper.

Conclusions

We have developed a CARS probe by encapsulating 200-nm polystyrene nanoparticles into folate-targeted liposomes and used this probe to study folate-receptor-mediated endocytosis in KB cells. By tuning $(\omega_p - \omega_s)$ to 3045 cm^{-1} , corresponding to the aromatic C–H stretching vibration, the polystyrene nanoparticles were selectively visualized with a high signal-to-noise ratio, while the epi-detected CARS signal from organelles was cancelled by the destructive interference between the resonant contribution from the aliphatic C–H vibration and the nonresonant contribution. Without photobleaching, endosome

transport could be investigated through single-particle tracking analysis of the CARS signal. No photodamage to cells was observed under our experimental conditions. The demonstrated advantages of using CARS probes to study dynamic processes in live cells provided a new direction for the application of CARS microscopy as a noninvasive biological imaging tool.

Acknowledgment. This work was supported by NIH Grant R21 EB004906 and NSF Grant #0416785-MCB.

References and Notes

- (1) Pawley, J. B. *Handbook of Biological Confocal Microscopy*; Plenum: New York, 1995.
- (2) Denk, W.; Strickler, J. H.; Webb, W. W. *Science* **1990**, *248*, 73.
- (3) Hurlley, S. M.; Helmuth, L. *Science* **2003**, *300*, 75.
- (4) Michalet, X.; Pinaud, F. F.; Bentolila, L. A.; Tsay, J. M.; Doose, S.; Li, J. J.; Sundaresan, G.; Wu, A. M.; Gambhir, S. S.; Weiss, S. *Science* **2005**, *307*, 538.
- (5) Larson, D. R.; Zipfel, W. R.; Williams, R. M.; Clark, S. W.; Bruchez, M. P.; Wise, F. W.; Webb, W. W. *Science* **2003**, *300*, 1434.
- (6) Dubertret, B.; Skourides, P.; Norris, D. J.; Noireaux, V.; Brivanlou, A. H.; Libchaber, A. *Science* **2002**, *298*, 1759.
- (7) Derfus, A. M.; Chan, W. C. W.; Bhatia, S. N. *Nano Lett.* **2004**, *4*, 11.
- (8) Cheng, J.-X.; Jia, Y. K.; Zheng, G.; Xie, X. S. *Biophys. J.* **2002**, *83*, 502.
- (9) Evans, C. L.; Potma, E. O.; Puoris'haag, M.; Cote, D.; Lin, C. P.; Xie, X. S. *Proc. Natl. Acad. Sci. U.S.A.* **2005**, *102*, 16807.
- (10) Cheng, J. X.; Xie, X. S. *J. Phys. Chem. B* **2004**, *108*, 827.
- (11) Volkmer, A. *J. Phys. D: Appl. Phys.* **2005**, *38*, R59.
- (12) Wang, H.; Fu, Y.; Zickmund, P.; Shi, R.; Cheng, J. X. *Biophys. J.* **2005**, *89*, 581.
- (13) Huff, T. B.; Cheng, J. X. *J. Microsc.* **2007**, *225*, 175.
- (14) Cheng, J. X.; Volkmer, A.; Book, L. D.; Xie, X. S. *J. Phys. Chem. B* **2001**, *105*, 1277.
- (15) Volkmer, A.; Cheng, J. X.; Xie, X. S. *Phys. Rev. Lett.* **2001**, *87*, 023901.
- (16) Potma, E. O.; Xie, X. S. *J. Raman Spectrosc.* **2003**, *34*, 642.
- (17) Li, L.; Wang, H.; Cheng, J.-X. *Biophys. J.* **2005**, *89*, 3480.
- (18) Müller, M.; Schins, J. M. *J. Phys. Chem. B* **2002**, *106*, 3715.
- (19) Potma, E. O.; de Boeij, W. P.; van Haastert, P. J. M.; Wiersma, D. A. *PNAS* **2001**, *98*, 1577.
- (20) Nan, X.; Potma, E. O.; Xie, X. S. *Biophys. J.* **2006**, *91*, 728.
- (21) Wurpel, G. W. H.; Schins, J. M.; Müller, M. *J. Phys. Chem. B* **2004**, *108*, 3400.
- (22) Potma, E. O.; Xie, X. S. *Chem. Phys. Chem.* **2005**, *6*, 77.
- (23) Leamon, C. P.; Low, P. S. *Proc. Natl. Acad. Sci. U.S.A.* **1991**, *88*, 5572.
- (24) Hilgenbrink, A. R.; Low, P. S. *J. Pharm. Sci.* **2005**, *94*, 2135.
- (25) Sudimack, J.; Lee, R. J. *Adv. Drug Deliv. Rev.* **2000**, *41*, 147.
- (26) Lee, R. J.; Low, P. S. *J. Biol. Chem.* **1994**, *269*, 3198.
- (27) Saul, J. M.; Annapragada, A.; Natarajan, J. V.; Bellamkonda, R. V. *J. Controlled Release* **2003**, *92*, 49.
- (28) Zumbusch, A.; Holtom, G. R.; Xie, X. S. *Phys. Rev. Lett.* **1999**, *82*, 4142.
- (29) Guo, W.; Lee, T.; Sudimack, J.; Lee, R. J. *J. Liposome Res.* **2000**, *10*, 179.
- (30) Galneder, R.; Kahl, V.; Arbutova, A.; Rebecchi, M.; Radler, J. O.; McLaughlin, S. *Biophys. J.* **2001**, *80*, 2298.
- (31) Crocker, J. C.; Grier, D. G. *J. Colloid Interface Sci.* **1996**, *179*, 298.
- (32) Hopt, A.; Neher, E. *Biophys. J.* **2001**, *80*, 2029.
- (33) König, K.; Becker, T. W.; Fischer, P.; Riemann, I.; Halbhuber, K. *J. Opt. Lett.* **1999**, *24*, 113.
- (34) Vogel, A.; Noack, J.; Huettmann, G.; Paltauf, G. *Proc. SPIE* **2002**, *4633A*, 1.
- (35) Fu, Y.; Wang, H.; Shi, R.; Cheng, J. X. *Opt. Express* **2006**, *14*, 3942.
- (36) Wang, H.; Fu, Y.; Cheng, J. X. *J. Opt. Soc. Am. B* **2007**, *24*, 544.
- (37) Martin, D. S.; Forstner, M. B.; Kaš, J. A. *Biophys. J.* **2002**, *83*, 2109.
- (38) Wang, H.; Huff, T. B.; Zweifel, D. A.; He, W.; Low, P. S.; Wei, A.; Cheng, J.-X. *Proc. Natl. Acad. Sci. U.S.A.* **2005**, *102*, 15752.
- (39) Durr, N. J.; Larson, T.; Smith, D. K.; Korgel, B. A.; Sokolov, K.; Ben-yakar, A. *Nano Lett.* **2007**, *7*, 941.
- (40) Chou, C.-H.; Chen, C.-D.; Wang, C. R. C. *J. Phys. Chem. B* **2005**, *109*, 11135.
- (41) Cheng, J. X.; Potma, E. O.; Xie, X. S. *J. Phys. Chem. A* **2002**, *106*, 8561.